

Synthesis of Zinc Ferrites in RF Thermal Plasma Reactor

L. Gál^{1*}, I. Mohai¹, I. Mészáros³, J. Gubicza⁴, J. Szépvölgyi^{1,2}

¹Institute of Materials and Environmental Chemistry, CRC HAS,
H-1525 POB 17, Budapest, Hungary

²Research Institute of Chemical and Process Engineering, University of Pannonia,
H-8200 POB 158, Veszprém, Hungary

³Research Group for Metals Technology, HAS-BME
H-1521 POB 91, Budapest, Hungary

⁴Department of Solid State Physics, Eötvös University,
H-1518 POB 32, Budapest, Hungary

Abstract

Formation of nanosized zinc ferrite spinels was studied from iron- and zinc oxide powders and corresponding nitrate solutions, respectively in a radiofrequency thermal plasma reactor. From the viewpoint of applications, the research was motivated by the potential use of these materials in advanced magnetic devices on the one hand, and by their biomedical applications such as drug carriers or agents for cancer treatment by hyperthermia on the other. In this work effects of synthesis conditions on properties of products were studied in details. The products were characterised for chemical composition, phase conditions, particle size distribution, morphologies and saturation magnetisation. Most products exhibited ferrimagnetic behaviour. Correlations among domain- and particle sizes were also investigated. Conditions for the synthesis of nanosized, inverse zinc ferrites of high saturation magnetisation were established. It was proved that in thermal plasma conditions normal and inverse ferrites could be produced in a single step process.

Keywords: zinc ferrites, RF thermal plasma, nanopowders

Introduction

Spinel ferrites of MeFe_2O_4 composition (where $\text{Me} = \text{Zn}^{2+}, \text{Fe}^{2+}, \text{Ni}^{2+}, \text{Co}^{2+}, \text{Cd}^{2+}, \text{Mg}^{2+}, \text{Mn}^{2+}$ etc.) are widely used as desulfurisation agents of flue gases from power plants, also as catalysts [1], material of electronic- and magnetic data recorder devices [2,3], gas sensors [4], microwave tools [5], magneto-optical equipments [6], drug carriers [7] and materials for cancer treatment [8]. Ferrite devices in electrical engineering and electronics are usually produced from ferrite powders by shaping and subsequent high temperature sintering. Ferrite powders are usually prepared by one of the following methods: (i) heat treatment of intimate mixtures of constituting oxides, (ii) precipitation of suitable hydroxides and (iii) sol-gel processing.

Another option is the vapour phase oxidation of liquid precursors such as metal-nitrate solutions at high temperatures. In this process the first step is the evaporation

of the solvent followed by the oxidation of nitrates and ferrite formation [9]. By setting the synthesis conditions properly, the evaporation, the chemical reaction and the condensation of products from the gas phase take place very rapidly, and fine-sized powders are formed. Zinc-ferrite spinels of ZnFe_2O_4 composition belong to the $Fd3m$ crystal group and crystallise in face-centred cubic structure. In the normal ferrites (Fig. 1) the Zn^{2+} ions are in tetrahedral positions, while the Fe^{3+} ions in octahedral ones; the O^{2-} ions are located among the lattice points [10]. The normal zinc-ferrite spinels have very low, actually zero resultant magnetic momentums. Below the Néel temperature (10K) ZnFe_2O_4 is antiferromagnetic, while at higher temperatures it is paramagnetic. However, in special conditions, e.g. on very intensive grinding or on heat treatment for several hours, a lattice inversion may occur. Some Zn^{2+} ions occupy octahedral positions and some Fe^{3+} ions tetrahedral ones. Thus, a so-called inverse zinc-ferrite structure being metastable in thermodynamic terms is formed with a composition of $(\text{Fe}^{3+}_x)(\text{Zn}^{2+}\text{Fe}^{3+}_{2-x})\text{O}_4$. The smaller is the particle size, the easier the formation of inverse structure. The inverse zinc-ferrite spinels are ferrimagnetic materials.

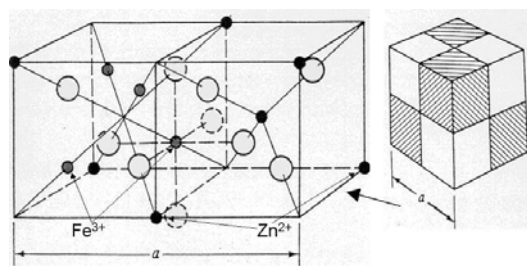


Fig. 1 The crystal lattice of normal zinc ferrite

The normal zinc ferrites are produced by one of the above listed more or less “traditional” methods. In order to get a material of inverse zinc ferrite structure, an extra energy input is required by intensive grinding [11] or mechanochemical activation of oxide mixtures [11]. It is known that in thermal plasma reactors special conditions such as very high temperatures, high energy densities and very high heating and cooling rates can be ensured. Such conditions may be favorable for the synthesis of inverse spinels, as well.

Research work presented in this paper was aimed at studying the synthesis of normal and inverse spinel ferrites in a radiofrequency thermal plasma reactor.

Experimental

The experiments aiming at synthesizing ferrites were performed in a radiofrequency thermal plasma reactor operating with a TEKNA PL-35 induction plasma torch at a maximum plate power of 30 kW. The experimental set-up is shown in Fig. 2. Argon was used as plasma gas with a flow rate of 20 l·min⁻¹. The sheath gas was a mixture of Ar and O₂ with flow rates of 23 l·min⁻¹ and 20 l·min⁻¹, respectively.

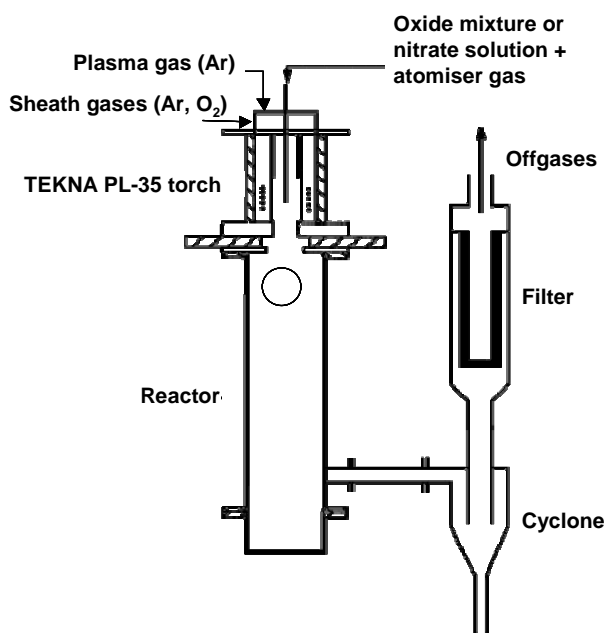


Fig. 2 Scheme of the experimental set-up

In this work the following precursors were tested: (1) mixture of ZnO and Fe₂O₃ powders with molar ratio of 1:2 and particle size of some micrometers and (2) ethanol solution of Zn(NO₃)₂·6H₂O and Fe(NO₃)₃·9H₂O with molar ratio of 1:2. The concentration of Zn²⁺ in the solution was 0.65 mol·dm⁻³.

The solid precursors were injected by a PRAXAIR powder feeder, while the nitrate solutions were injected by a TEKNA suspension feeder into different zones of the plasma flame. The feeding points are shown in Fig. 3. In all cases Ar (3 l·min⁻¹) was used as carrier and atomization gas, respectively.

Conditions of ferrite synthesis and properties of products are listed in Table 1. The reaction products were mainly collected from the water-cooled wall of the reactor.

The particle size distribution of ferrites was determined by laser-diffraction (Malvern Mastersizer 2000). Morphology of products was studied by SEM (Philips XL30 ESEM) and TEM (Philips CM20). Energy dispersive X-ray fluorescence spectroscopy (EDS; NORAN EDS) was applied to analyse the Fe and Zn content of individual particles.

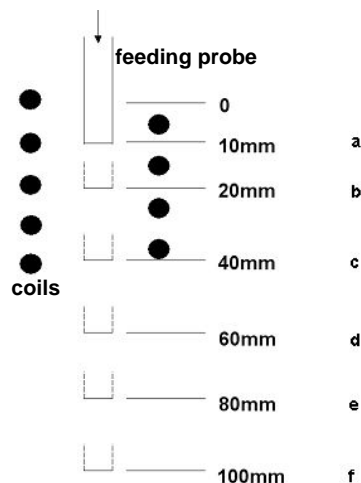


Fig. 3 Feeding points of powders and solutions, respectively

The chemical composition of ferrite powders was analysed by ICP-OES (Thermo Jarrell Ash Atomscan 25). A Philips Xpert XRD apparatus operating with Cu K_α radiation was used to determine the phase composition and domain sizes. The lattice parameter ((a) in Fig. 1) of the crystalline phases was determined from the positions of relevant diffraction peaks. Composition of spinel structure was determined by deconvoluting the 731 spinel reflection of X-ray diffractograms (Fig. 4).

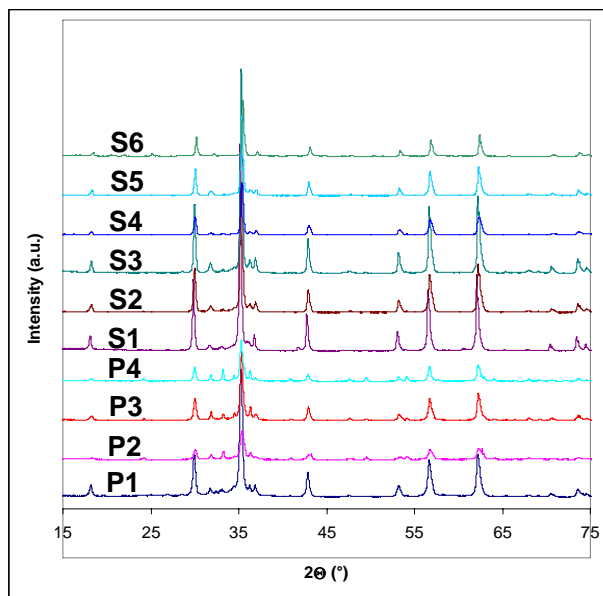


Fig. 4 XRD patterns of ferrites. For legends see Table 1.

Investigations on magnetic properties

A specially designed vibrating sample magnetometer (VSM) was applied for measuring the first magnetization curves of samples. The basic principle of VSM is that if a material is placed into magnetic field a dipole moment will be induced in it, which is proportional to the susceptibility of the material and the intensity of the applied magnetic field. If the sample produces sinusoidal vibration, changes in the magnetic flux near to the sample will induce an electrical signal in the suitably

placed detector coils. The induced voltage is proportional to the magnetic moment of the sample, the amplitude and frequency of the vibration. Using a vibration controlling reference coil the amplitude and frequency dependence can be eliminated and the instrument can be calibrated.

The VSM instrument used in this work was designed and constructed at the Department of Materials Science and Engineering of BME. In contrast to the traditional so called Foner-type magnetometers, in this VSM instrument the specimen vibrates along the external magnetizing field. Therefore, it is called parallel motion vibrating sample magnetometer (PMVSM). This parallel motion arrangement has several advantages like increased sensitivity, better signal to noise ratio, simpler detector coil arrangement and easier specimen positioning. The equipment is PC controlled and it quasi-statically drives the laboratory electromagnet. The vibration-driving signal was sinusoidal with frequency of

75 Hz. The system was calibrated by using a nickel sphere as a standard.

For the ferrite powder samples a special cylindrical specimen holder was designed. The investigated powders were compacted by pressing into the specimen holder. The sample volume was 650 ± 200 mg depending on the specific weight and the compactness of powders.

The initial magnetization $M(H)$ curves were measured by magnetizing the samples up to about $5000 \text{ A}\cdot\text{cm}^{-1}$ external field. The complete magnetic saturation of the samples was achieved at about $2000 \text{ A}\cdot\text{cm}^{-1}$. The specimens contained significant amount of paramagnetic and ferrimagnetic phases. The contribution of the paramagnetic phase was eliminated from the magnetization curves. Thus, the actual specific saturation magnetization of ferrimagnetic phases was determined.

Table 1 Experimental conditions and properties of products

Precursor	ZnO + Fe ₂ O ₃				Zn(NO ₃) ₂ ·6H ₂ O + Fe(NO ₃) ₃ ·9H ₂ O					
Run No.	P1	P2	P3	P4	S1	S2	S3	S4	S5	S6
Experimental conditions										
Position of feeder	a	a	b	b	a	b	c	d	e	f
Plate power (kW)	25	15	25	15	15	15	15	15	15	15
Feed rate of solid precursors (g·h ⁻¹)	7.86	17.7	21.6	27.7	298	289	247	320	265	256
Specific energy (kWh·g ⁻¹)*	3.11	0.87	1.16	0.57	0.05	0.05	0.06	0.05	0.06	0.06
Properties of products										
Powder yield (weight %)	24	17	22	17	33	29	42	20	30	38
d ₅₀ (l) (nm)	78	77	349	72	115	75	163	463	356	369
Relative magnetite content (%)	44	35	46	0	8	4	27	18	58	32
Saturation magnetisation (emu·g ⁻¹)	28	30	36	19	7	7	9	10	14	18
Domain size of zinc ferrite (nm)	25	26	76	53	46	51	54	57	61	61
Domain size of magnetite (nm)	100	100	62	0	30	30	17	19	22	30

* related to solid precursors

Results and discussion

The experimental conditions and the properties of products are summarized in the Table 1. The specific energy was defined as the ratio of plate power against the feed rate of precursors. It can be regarded as an overall parameter of powder synthesis.

Chemical composition of ferrites determined by ICP-OES method are not listed in Table 1, because in all cases ferrite powders of targeted composition (Zn : Fe = 1 : 2) were produced.

The powder yields calculated from the amount of product collected from the reactor wall and from the theoretical value assuming a 100 % conversion of precursors to ferrites are relatively low (17 - 42 %). It is mainly reasoned by the poor efficiency of powder separation from the voluminous gas phase in the reac-

tor due to the small particle size of the products. The nanosized ferrite particles were mainly separated in the reactor by thermophoresis being not enough intensive in particular conditions. The highest yield of 42 % was obtained when precursor nitrate solution was fed just at the lower level of induction coil (Run No. S3).

The morphology of ferrite powders was characterized by d₅₀ values obtained from laser diffraction measurements (Table 1). In all tests nanosized powders were formed. However, the characteristic size of ferrite particles depends in a complex way on the size of precursor, its feeding point and the specific energy, as well.

The SEM (Fig. 5) and TEM (Fig 6) micrographs support the results of PSA analyses. Nanosized, spherical particles were formed which were inclined to agglomeration. However, they formed loose agglomerates that can be disintegrated with ease by ultrasonic agitation at a power of 20 W for several minutes. The EDS meas-

measurements showed a small excess of Zn in the smaller particles and excess of Fe in the larger ones. Grains of optimum stoichiometry had a mean size of 60-80 nm. In all Runs the main crystalline phase of the powders was zinc ferrite (Fig. 3). However, some magnetite was also detected by XRD. Beside zinc ferrite and magnetite, some zincite and hematite were formed, as well. The relative magnetite content in Table 1 was calculated from the XRD patterns as the ratio of magnetite content against zinc ferrite content of ferrite powders. In the case of oxide precursors the relative magnetite content varied from 0 to 46 %, while in the nitrate case from 4 to 58 %.

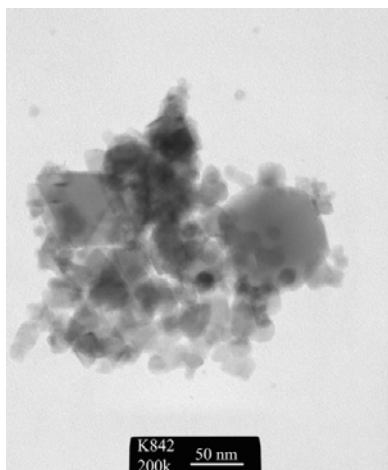


Fig. 5 TEM micrograph of Sample S3

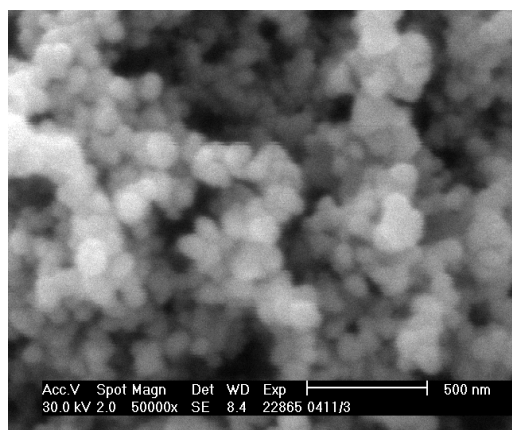


Fig. 6 SEM micrograph of Sample S3

Apart from Runs P4 and S5, relatively less magnetite was formed from the nitrate solutions than from the oxide mixtures. (We have to remark that the specific energy was much higher in the oxide case due to experimental conditions.) The lower relative magnetite content of powders produced from nitrates is explained by the more homogeneous distribution and thus, the more intimate contact of zinc- and iron-containing species in the ethanol solution, and also in the plasma flame. It decreases the chance of magnetite formation. According to data of Table 1 the saturation magnetization is closely connected to the magnetite content of products. However, in Run P4 a relatively high saturation magnetization was detected in spite of the absence

of magnetite. It refers to formation of inverse spinel structure.

The domain size of zinc ferrite crystallites is in the range of 25 to 76 nm, while that of magnetite crystallites varies from 17 to 100 nm. These sizes are comparable with the d_{50} values that support further evidence on the very rapid cooling of primary grains below the plasma flame region.

Our results suggest that the distribution and thus, the thermal history of precursors and the as-synthesized particles, respectively, in the plasma flame have a decisive effect on the morphology, phase composition and hence, magnetic properties of particular powders.

A graphical summary of the results of particular work for the oxide precursors is shown in Fig. 7, while for the nitrate case in Fig. 8. All data are plotted in logarithmic scale with maximum values of 1000.

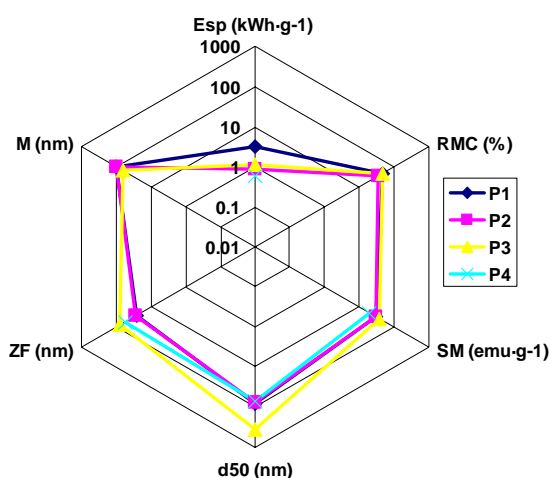


Fig. 7 Summary of the experimental results for oxide precursors. Esp: Specific energy, RMC: Relative magnetite content, SM: Saturation magnetization, d_{50} : $d_{50}(I)$, ZF: zinc ferrite domain size, M: magnetite domain size

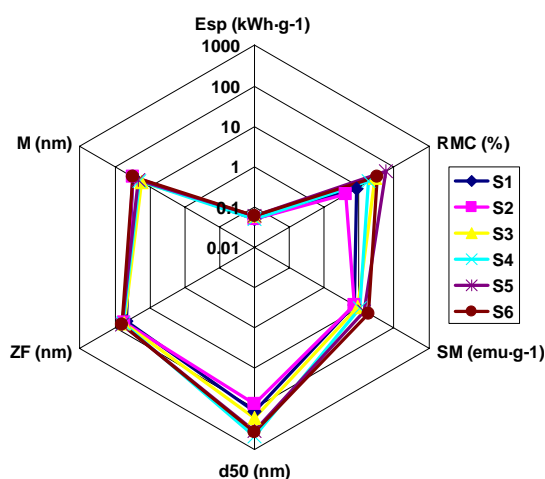


Fig. 8 Summary of the experimental results for nitrate precursors. Esp: Specific energy, RMC: Relative magnetite content, SM: Saturation magnetization, d_{50} : $d_{50}(I)$, ZF: zinc ferrite domain size, M: magnetite domain size

In powder case, the specific energies are higher with an order of magnitude as compared to nitrate precursors. The relative magnetite contents of samples produced from nitrates are changing in a broader range than that of products from oxides. The saturation magnetizations of Samples P1-P4 are a little bit higher, than that of others. It is traced back to the zinc ferrite inversion and the higher relative magnetite content, respectively. Mean particle- and domain sizes do not differ remarkably. However, the magnetite domain size is slightly larger in the case of oxide precursors.

Conclusions

It has been proved that nanosized normal and inverse spinel zinc ferrites were produced in a radiofrequency thermal plasma reactor both from the mixture of relevant oxides and the ethanol solution of zinc and iron nitrates. Particle size, phase composition and magnetic properties of products depend on the properties of precursors on the one hand, and on the synthesis conditions on the other. The thermal history of the reactive species has a decisive effect on the morphology, phase composition and hence, magnetic properties of zinc-ferrite powders.

References

1. Yürüm, Y. (ed): Clean Utilization of Coal: Coal Structure and Reactivity, Cleaning and Environmental Aspects, Kluwer, 1992, NATO ASI Series 370, pp. 221.
2. Sugita N., Maekawa M., Ohta Y.: Advances in Fine Magnetic Particles for High-Density Recording - IEEE Transactions on Magnetics **31** (1995) 2854.
3. Oliver, S. A., Yoon, S.D., Kozulin, I.: Growth and Characterization of Thick Oriented Barium Hexaferrite Films on MgO (111) Substrates - Applied Physics Letters **76** (2000) 3612.
4. Sandu, I., Presmanes, L., Alphonse, P., Tailhades, P.: Nanostructured Cobalt Manganese Ferrite Thin Films for Gas Sensor Application - Thin Solid Films **495** (2006) 130.
5. Fu, Y. P., Hsu, Ch. Hs.: Microwave-Induced Combustion Synthesis of $\text{Li}_{0.5}\text{Fe}_{2.5-x}\text{Mn}_x\text{O}_4$ Powders and their Characterization - Journal of Alloys and Compounds **391** (2005) 185.
6. Gut, B. X., Zhang, H. Y., Zhai, H. R.: Physics of Condensed Matters **6** (1994) 1047.
7. S. Rana, A. Gallo, R.S. Srivastava and R.D.K. Misra: On the suitability of nanocrystalline ferrites as a magnetic carrier for drug delivery: Functionalization, conjugation and drug release kinetics - Acta Biomaterialia, **3** (2007) 233.
8. P. Pradhan, J. Giri, R. Banerjee, J. Bellare and D. Bahadur Preparation And Characterization of Manganese Ferrite-Based Magnetic Liposomes for Hyperthermia Treatment of Cancer - Journal of Magnetism and Magnetic Materials, **311** (2007) 208.
9. Economos, G.: Magnetic Ceramics: I, General Methods of Magnetic Ferrite Preparation - Journal of the American Ceramic Society, **38** (1955) 241.
10. Cullity B. D. - Introduction to Magnetic Materials, Addison-Werley, Reading, MA (1972).
11. Druska, P., Steinike, U., Sepelák, V.: Surface Structure of Mechanically Activated and of Mechanothesized Zinc Ferrite - Journal of Solid State Chemistry **146** (1999) 13.
12. Mészáros, I.: Micromagnetic Measurements and their Applications - Materials Science Forum **414** (2003) 275.